nature COMMUNICATIONS

ARTICLE

Received 5 Aug 2015 | Accepted 10 May 2016 | Published 10 Jun 2016

DOI: 10.1038/ncomms11892 OPEN

Interfacial control of oxygen vacancy doping and electrical conduction in thin film oxide heterostructures

Boyd W. Veal[1], Seong Keun Kim[1,†], Peter Zapol[1], Hakim Iddir[1], Peter M. Baldo[1] & Jeffrey A. Eastman[1]

Oxygen vacancies in proximity to surfaces and heterointerfaces in oxide thin film heterostructures have major effects on properties, resulting, for example, in emergent conduction behaviour, large changes in metal-insulator transition temperatures or enhanced catalytic activity. Here we report the discovery of a means of reversibly controlling the oxygen vacancy concentration and distribution in oxide heterostructures consisting of electronically conducting In_2O_3 films grown on ionically conducting Y_2O_3-stabilized ZrO_2 substrates. Oxygen ion redistribution across the heterointerface is induced using an applied electric field oriented in the plane of the interface, resulting in controlled oxygen vacancy (and hence electron) doping of the film and possible orders-of-magnitude enhancement of the film's electrical conduction. The reversible modified behaviour is dependent on interface properties and is attained without cation doping or changes in the gas environment.

[1] Materials Science Division, Argonne National Laboratory, Argonne, Illinois 60439, USA. † Present address: Center for Electronic Materials, Korea Institute of Science and Technology, Seoul 136-791, South Korea. Correspondence and requests for materials should be addressed to J.A.E. (email: jeastman@anl.gov).

The discoveries of a wide range of remarkable behaviours in thin film oxide heterostructures have led to intense interest in their synthesis and characterization. Oxygen vacancy concentrations exceeding bulk levels near surfaces and interfaces have recently been cited as instrumental in controlling these behaviours. For example, large changes in electrical resistance associated with metal-insulator transitions[1,2] or resistive switching behaviour[3,4] have been linked to increased oxygen vacancy concentrations in thin film heterostructures. Magnetism in thin film heterostructures of bulk non-magnetic materials[5,6] has been attributed to the presence of oxygen vacancies near interfaces[7–10], and catalytic activity of oxide heterostructures has been explained by enhanced interfacial oxygen vacancy concentrations[11–16]. Also, localized metallic conduction has been reported near heterointerfaces between bulk oxide insulators (e.g., $LaAlO_3/SrTiO_3$)[17]. While the origin of this remarkable conduction behaviour is the subject of continuing debate, several authors have concluded that it is caused by oxygen vacancy doping of $SrTiO_3$ substrates during thin film deposition[18–22].

These examples demonstrate the importance of being able to manipulate oxygen vacancies to achieve emergent behaviour, motivating the exploration of new ways to control vacancy concentrations and distributions in oxide thin film heterostructures. In this study, we investigated the possibility of using electric fields to control oxygen vacancies in model thin film heterostructures, primarily epitaxial thin films of In_2O_3 grown on (001) and (111) surfaces of Y_2O_3-stabilized ZrO_2 (YSZ).

In the following, we show that, when a small in-plane electric field is applied to In_2O_3-on-YSZ heterostructures, the measured electrical conductance rises dramatically, in some cases by more than two orders-of-magnitude. The question thus arises: How do electrons and ions in these heterostructures interact to produce this remarkable phenomenon? We show that the effect arises from the response to resistances that develop at the electrodes following application of the in-plane field.

Results

Field-induced conductance increase. Epitaxial In_2O_3 films were deposited on single crystal (001) YSZ, (111) YSZ or (001) $MgAl_2O_4$ substrates. The <2% misfit strain between bixbyite-structured In_2O_3 and fluorite-structured YSZ enables the growth of epitaxial single crystal films with a cube-on-cube orientation relationship between the film and substrate[23–25]. In_2O_3 is an oxide semiconductor, exhibiting n-type conductivity[26,27] (see Supplementary Fig. 1 and Supplementary Note 1). In contrast, YSZ is a fast oxygen ion conductor with negligible electronic conductivity[28]. Oxygen ions in the ionically conducting YSZ substrate will migrate in an electric field, with oxygen vacancies moving towards the negative electrode. Oxygen ions enter YSZ at triple phase boundaries at the negative electrode according to $O_2(g) + 2V_O^{\cdot\cdot} + 4e' \rightarrow 2O_O^x$, which is written using Kröger-Vink notation[29], where $V_O^{\cdot\cdot}$ indicates an oxygen vacancy with a $+2$ charge, e' is an electron and O_O^x is an oxygen ion with a formal -2 valence sitting in an oxygen lattice site. Oxygen exits the sample at the positive electrode by the reverse reaction.

Electrical characterization was performed on samples with the electrode geometry shown in Fig. 1. We monitored the conductance response when small DC fields were applied in the plane of the film by flowing current between electrodes 1 and 7 while monitoring the voltage using a pair of electrodes on the surface of the film (shown as 5 and 6 in Fig. 1). Surprisingly, all samples grown on YSZ that were exposed to small DC fields showed a monotonic rise in conductance with time, such as is shown in Fig. 2. In this particular case, with a field of $\sim 4\,V\,cm^{-1}$ applied, the conductance increased by a factor of nearly 200 relative to the starting (zero field) value.

The conductance enhancement was found to be reversible, with the conductance returning to approximately the original value after removal of the field. The relative change in conductance was observed to increase with decreasing film thickness (see Supplementary Table 1). This indicates that the field-induced conduction enhancement is localized to a region in the films near the film/substrate heterointerface.

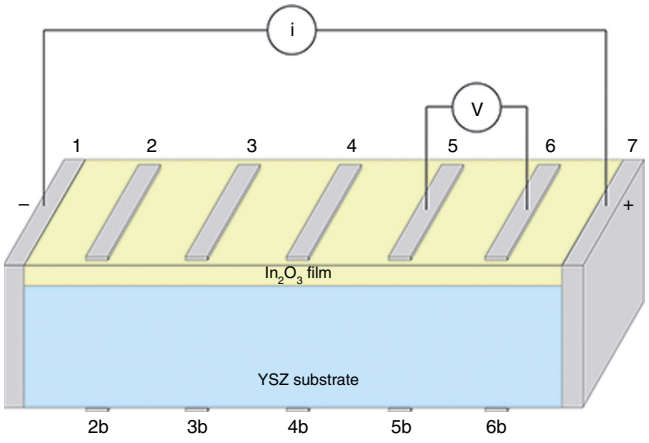

Figure 1 | Sample schematic. Equally spaced Pt parallel line electrodes (voltage pick-offs) were sputter-deposited through a shadow mask on the films (numbered 2–6) and, for some samples, on the other surface of the YSZ substrate (2b-6b). The current electrodes (numbered 1 and 7) were Ag or Pt paint.

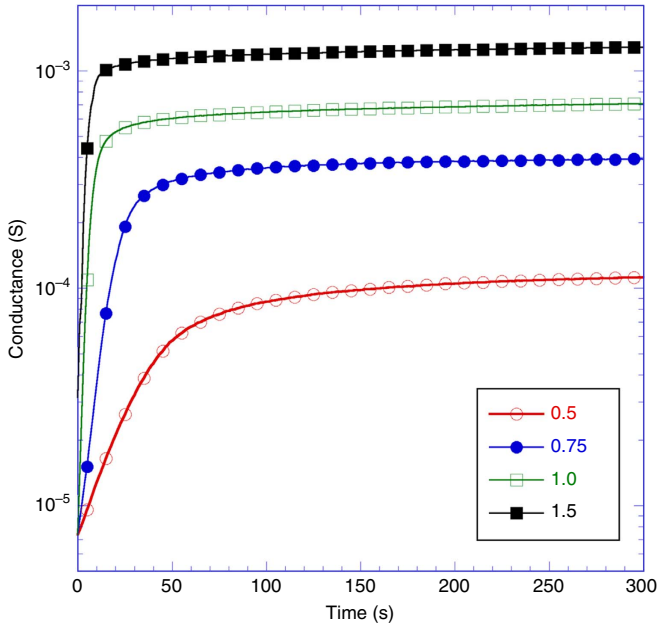

Figure 2 | Field-induced electrical conductance increase. Time-dependent increases in conductance were observed at different measurement voltages. Voltage V_{23} was held constant at the values indicated in the legend (in Volts), while flowing current between electrodes 1 and 7. The electrode configuration is shown in Fig. 1. The conductance is enhanced by a factor of 190 at the highest voltage (field) shown. The measurements were taken at 370 °C, with the sample equilibrated at $pO_2 = 150$ torr.

Responses of interfaces to applied fields. Further experiments were carried out to determine the mechanism responsible for the observed field-induced conductance increases. These measurements clearly demonstrate that the dramatic enhancement of the sample conductance is determined by the response of multiple interfaces in the heterostructure to the application of small electric fields. There are five relevant interfaces in the heterostructure. In addition to the planar YSZ/In_2O_3 interface, Ag/YSZ and Ag/In_2O_3 interfaces (or Pt/YSZ and Pt/In_2O_3 interfaces), at both positive and negative electrodes, must be considered. Pt/In_2O_3 interfaces at the voltage pickoffs do not contribute to the observed behaviour, since a four-electrode configuration is used and pick-off voltages are measured with a high input impedance voltmeter.

When a DC field is applied between the end electrodes (electrodes 1 and 7 in Fig. 1), a voltage profile is established laterally across the sample. If there are no contact resistances, and samples are homogeneous, the profiles across the In_2O_3 and YSZ are identical. However, if contact resistances at the electrode/film and electrode/substrate interfaces differ, the lateral voltage profile across the In_2O_3 film can be different from that across the YSZ substrate. This can happen because YSZ is an ionic conductor and In_2O_3 is an electronic conductor. Figure 3a shows measured voltage profiles across a bare substrate and a thin film heterostructure, with Pt end electrodes, at time $t = 0$, when the DC field is first applied. Figure 3b shows the profiles across the same two samples after relaxation to steady state has occurred. The initial profiles in Fig. 3a are nearly identical, indicating that all contact resistances are similar and small at time zero, when the voltage is first applied. However, at steady state, the profiles shown in Fig. 3b have dramatically diverged. A large resistance has developed at the negative Pt electrode/YSZ interface, where oxygen entry occurs. The resistance at the positive Pt electrode/YSZ interface, where oxygen exit occurs, shows very little change with time. At the same time, a large resistance develops at the positive Pt electrode/In_2O_3 interface. No significant resistance develops at the negative Pt electrode/In_2O_3 interface. Supplementary Figs 2 and 3 show the time development of similar contact resistances when the end electrodes are Ag rather than Pt.

Electrochemical reactions associated with oxygen entry and exit are likely to be responsible for the time-dependent increases in resistance at the YSZ/metal electrode/environment triple junctions when a DC potential is applied. For example, time-dependent changes in the polarization resistance at Pt electrode/YSZ electrolyte/environment triple junctions have been reported in numerous studies and have often been linked with formation of nonstoichiometric PtO_x at the interface when a potential is applied[30–33]. This field-driven PtO_x formation may impede the oxygen exchange reactions $\left(O_2(g) + 2V_O^{\cdot\cdot} + 4e' \rightarrow 2O_O^x\right)$ that occur at the triple junctions[34], altering the contact resistances. While the electrochemistry of Ag/YSZ junctions in oxidizing environments has not been as extensively studied as Pt/YSZ, a similar impediment to oxygen exchange would be expected to occur if Ag electrodes in contact with the YSZ are oxidized at the triple junctions when a field is applied.

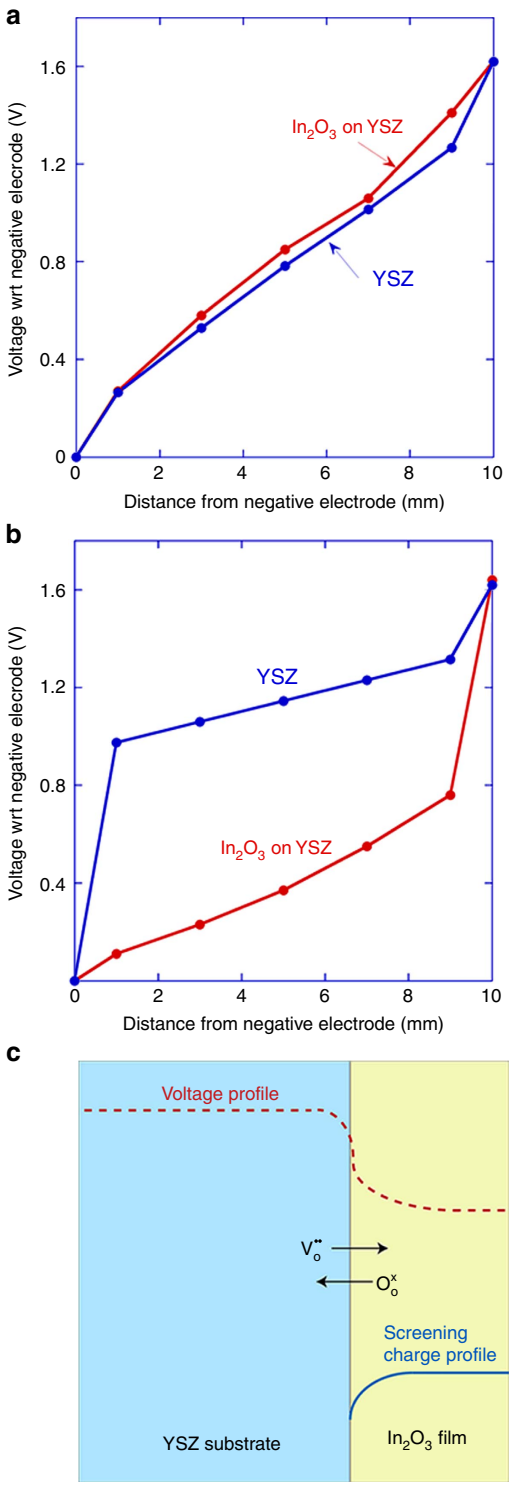

Figure 3 | Voltage profiles. (**a**) Initial voltage profile across a bare YSZ substrate compared with the profile across a 51 nm thick In_2O_3-on-YSZ sample when a 1.6 volt battery is connected to electrodes 1 and 7 at 330 °C (electrode configuration shown in Fig. 1). Minimal contact resistances are present initially. (**b**) The voltage profiles after 5 min (at steady state) for the same two samples. For the bare YSZ substrate, a large contact resistance has developed at the negative electrode (where oxygen entry occurs). A smaller contact resistance appears at the positive electrode (oxygen exit). A Schottky-type resistance appears at the positive electrode of the In_2O_3-on-YSZ sample. As a result of these resistances, a voltage drop develops between YSZ and the In_2O_3 film, with the substrate at a higher potential than the film. (**c**) The voltage profile that develops across the In_2O_3 /YSZ interface causes oxygen ions to move across the interface from In_2O_3 to YSZ. A screening charge appears in the In_2O_3 film near the interface. This interfacial electron doping increases the conductivity of the In_2O_3. In the YSZ, charge neutrality is maintained by mobile excess oxygen ions moving away from the interface.

The observed rectifying behaviour of the positive and negative electrode junctions with the film (Supplementary Fig. 3) may be associated with the formation of a Schottky barrier at the positive electrode/In_2O_3 interface, which has been reported to develop between In_2O_3 films and Pt electrodes when oxygen vacancies are eliminated from the region of the heterointerface[35]. In the current experiment, oxygen ions migrate towards the positive current electrode under the influence of the applied field, eliminating oxygen vacancies from the In_2O_3 film near the interface with the positive current electrode.

Voltage across the film/substrate interface. As a result of the changes in the interfacial resistances (primarily at the negative electrode/YSZ interface and at the positive electrode/In_2O_3 interface), which develop with field exposure, a substantial voltage drop appears between the YSZ substrate and the In_2O_3 film. The voltage drop is concentrated at the In_2O_3/YSZ interface, where ionic and electronic conductors meet, as illustrated in Fig. 3c. This component of the field, oriented normal to the interface, moves electrons in In_2O_3 and oxygen vacancies in YSZ towards the interface and provides a driving force to move oxygen ions from the film to the substrate. Enhanced electron doping of the In_2O_3 occurs within a relatively short distance, that is, a screening length of $\sim$10 nm from the interface, as discussed in Supplementary Note 2. While the detailed physical processes controlling the electrochemistry at the contacts remain under active investigation, for our purposes it is sufficient to monitor the development of the contact resistances following application of a DC voltage. Consideration of the time-dependent behaviour appears in Supplementary Figs 4 and 5 and Supplementary Note 1.

As seen in Fig. 4, the development of the potential across the In_2O_3/YSZ interface was confirmed by directly measuring the voltage between pairs of electrodes on the top and bottom surfaces of a sample as a function of time while again flowing current between electrodes 1 and 7. The voltage across the In_2O_3/YSZ interface was observed to increase from zero with time of field application, with YSZ at a higher potential than In_2O_3, consistent with the measurements shown in Fig. 3b.

Since a DC in-plane electric field imposes a voltage in a direction normal to the film/substrate interface, which drives oxygen ions from the In_2O_3 film into the YSZ substrate, we investigated whether a similar doping effect might be achieved by directly applying a voltage across the YSZ/In_2O_3 heterointerface. Figure 5 shows measurements when a voltage is applied between electrodes on the top and bottom surfaces of the sample using a battery, while the average conductance in the in-plane direction is measured between the end electrodes. We see that, consistent with our other observations, the average conductance increases when the substrate is at a higher potential than the substrate, while the conductance decreases when the voltage direction is reversed to place the substrate at a lower potential than the film.

Development of a conductance gradient. Figures 3b and 4 also show that the voltage drop between YSZ and the In_2O_3 film is larger near the negative current electrode than it is near the positive current electrode, suggesting that a conductance gradient will appear in the film. Figure 6a confirms this, showing the time dependence of the average conductance between adjacent

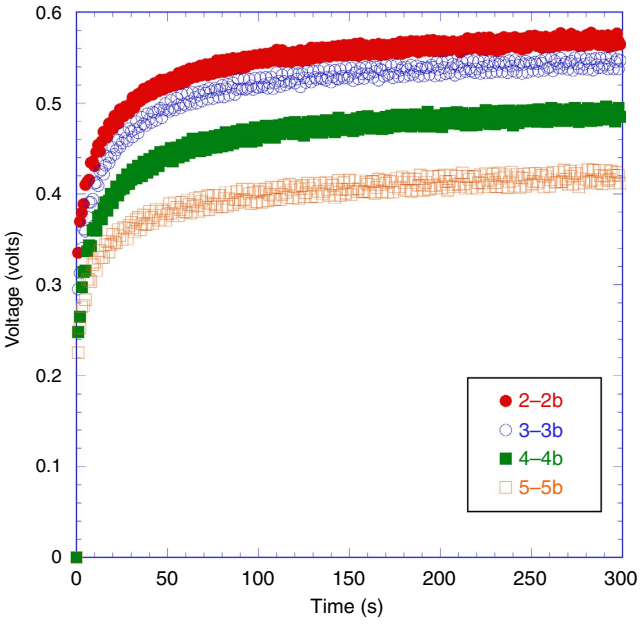

Figure 4 | Development of voltage across the film/substrate interface. The voltage drop measured between the film surface and the back surface of the substrate at four positions on a sample when an in-plane current of 5×10^{-5} Amps is imposed between electrodes 1 and 7 (see Fig. 1 for electrode configuration). The legend denotes the pairs of top/bottom electrodes used for each measurement. Measurements were taken at 370 °C, with the sample equilibrated at $pO_2 = 1.5$ torr.

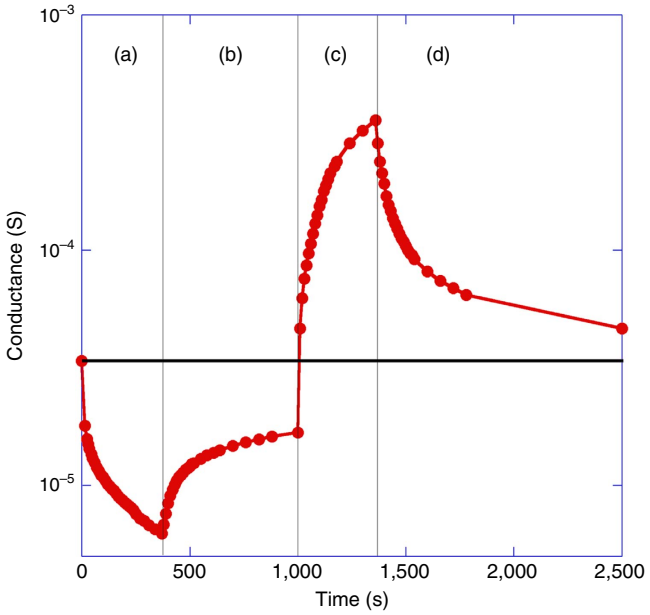

Figure 5 | Applying a voltage across the film/substrate interface. Measurements of the average conductance between electrodes 1 and 7, plotted versus time when a voltage is applied between electrodes 4 and 4b using a battery (see Fig. 1 for the electrode configuration). Region (a): Applying 1.6 V, with the film at a higher potential than the substrate, moves oxygen ions from YSZ into the In_2O_3. This reduces the oxygen vacancy doping of the film, thus reducing the measured conductance. Region (b): When the battery is open-circuited, the conductance relaxes towards the initial value as the film's oxygen vacancy concentration returns to the equilibrium value determined by the temperature and pO_2. Region (c): Applying 1.6 V, with the substrate at a higher potential than the film, moves oxygen ions from In_2O_3 into the YSZ. This oxygen vacancy dopes the film, thus increasing the measured conductance. Region (d): Removing the battery again results in the measured conduction relaxing towards the starting value as the film oxygen vacancy concentration returns to that set by the temperature and pO_2. The measurements were taken at 330 °C with $pO_2 = 1.5$ torr.

electrodes under constant current conditions. The largest conduction enhancement at steady state is observed when the voltage pick-off electrodes used are closest to the negative current electrode. Figure 6b shows the corresponding field-enhanced conductance values at steady state, as a function of position on the sample. As expected, the conductance is largest near the negative electrode and shows a gradient across the sample.

We note that electric field-induced polarization has been observed to occur in many different mixed oxide conductors (that is, oxides that exhibit both ionic and electronic conduction), a manifestation of the well-known Hebb-Wagner polarization mechanism[36,37]. Hebb-Wagner polarization occurs in mixed electron/ion conductors exposed to a DC field when ionic conduction is blocked by a current electrode. Resultant polarization of the mobile ions may in turn locally alter the electronic conductivity, producing an electronic conductivity gradient. Hebb-Wagner polarization is not observed in In_2O_3 or YSZ because these oxides are not mixed conductors. While, similar to Hebb-Wagner behaviour, we observe in-plane polarization (development of a conductivity gradient) when applying an in-plane DC field, the polarization mechanism observed here results from the development of different electric field profiles in the substrate and film, which is not a characteristic of the Hebb-Wagner mechanism. The electrical behaviour of the heterostructure, at steady state, is approximately represented by the equivalent circuit shown in Supplementary Fig. 6 and discussed in Supplementary Note 3.

Since the measured field-induced conductance enhancement depends on the distance of the voltage pick-off electrodes from the negative current electrode, it is expected that reversing the current direction, which changes that spacing and also reverses the conduction gradient, will result in a different steady state conductance being attained (unless the pick-off electrodes are symmetrically located with respect to the current electrodes, in which case the distance of the pick-off electrodes from the negative current electrode is not changed by reversing the current direction). Figure 7 shows measurements that confirm this behaviour. The current-reversal observations shown in Fig. 7 also rule out sample resistive heating as a cause of the field-induced enhanced conductance. Resistive heating would be independent of current direction, always acting to increase the conductance, and would not produce a gradient.

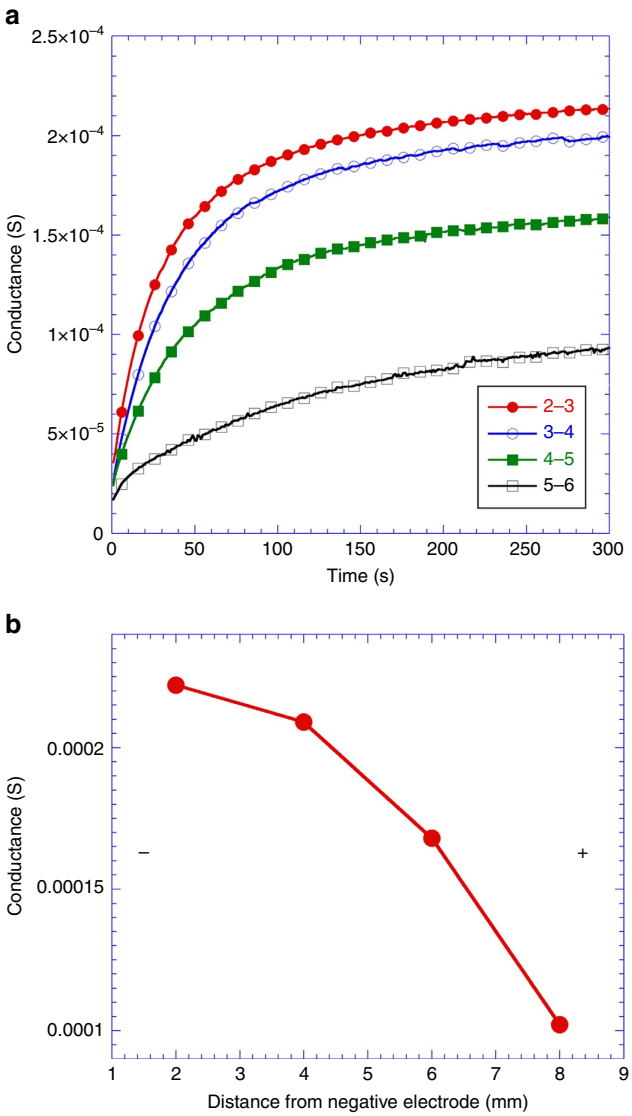

Figure 6 | Evidence of a conduction gradient. (**a**) Time dependence of conductance measured between adjacent pairs of voltage pick-off electrodes (denoted in the legend), with a constant current of 5E-5 amps flowing between electrodes 1 and 7 (see Fig. 1 for electrode configuration). Measurements were taken at 370 °C, with the sample equilibrated at $pO_2 = 1.5$ torr. (**b**) Conductance as a function of position on the sample, at steady state. The conductance is largest near the negative current electrode and shows a gradient across the sample.

Importance of the substrate and the film/substrate interface. Constant current measurements of conductance, with reversal of current direction, are also shown in Fig. 7 for an In_2O_3-on-$MgAl_2O_4$ sample. While the conductance of the In_2O_3 film grown on a $MgAl_2O_4$ substrate was observed to drift slightly with time due to slow equilibration of the sample under the

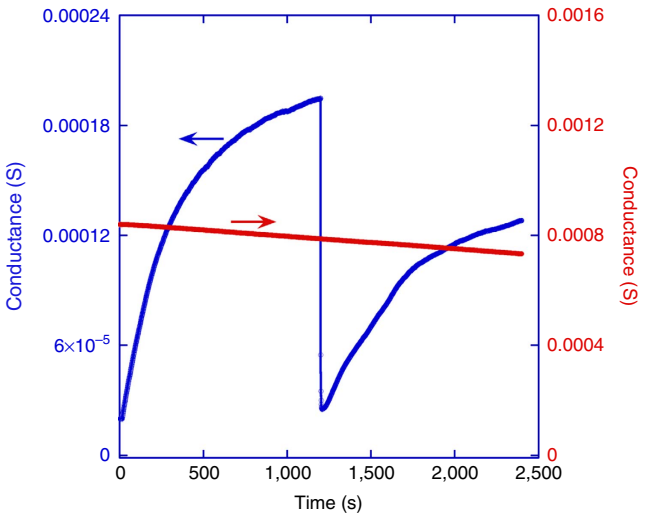

Figure 7 | Comparison of the behaviour of different substrates. Conductance versus time for In_2O_3 /YSZ (blue,) and In_2O_3 /$MgAl_2O_4$ (red) samples, under constant current conditions. The field was applied at $t = 0$, and the field direction was reversed for both samples at $t = 1{,}200$ s. Transient behaviour was observed for the In_2O_3 /YSZ sample, with the conductance evolving towards a different steady-state conductance for the two current directions. This behaviour occurs because the voltage pick-off electrodes are asymmetrically located with respect to the current electrodes. Since $MgAl_2O_4$ is not a fast oxygen ion conductor, the field application and reversal had no effects on the measured conductance of the In_2O_3 /$MgAl_2O_4$ sample. Both samples were measured at 330 °C with $pO_2 = 1.5$ torr.

temperature and oxygen partial pressure conditions used, no change in conductance was observed in response to application of a DC field, nor was a change in conductance observed when the field direction was reversed. These observations demonstrate that the substrate has a profound effect in determining whether field-induced changes in conduction occur, both in establishing the voltage component normal to the heterointerface that provides the driving force for ion motion, and in serving as a source/sink of mobile oxygen vacancies/ions. We hypothesize that $In_2O_3/MgAl_2O_4$ heterostructures do not show field-induced conduction enhancement because the substrate in this case is not a fast oxygen ionic conductor with a large oxygen vacancy concentration.

Since oxygen transport across the In_2O_3/YSZ interface is essential to the mechanism described here, we investigated the detailed structure and thermodynamics of the interface using first-principles calculations. In particular, we determined relative oxygen vacancy formation energies near the interface to evaluate the feasibility of the migration of oxygen vacancies into the In_2O_3 film from the YSZ substrate. We considered the (001) In_2O_3/YSZ and In_2O_3/ZrO_2 interfaces with atomic stacking normal to the interface that alternates between cation and oxygen planes, with a shared oxygen plane at the interface. Models were considered with different oxygen occupation of the interface plane, from O-deficient to O-rich (see Methods and Supplementary Figs 7 and 8). As seen in Fig. 8a, over a wide range of chemical potentials and corresponding T and pO_2 conditions, the formation energy of oxygen-deficient (001) In_2O_3/ZrO_2 interfaces is predicted to be lower than the formation energies of vacancies in either bulk material (6.06 eV for ZrO_2 and 4.05 eV for In_2O_3). The vacancy formation energy is possibly reduced at the interface compared with bulk because of the different oxygen stoichiometry and Madelung field on either side of the interface. Bulk ZrO_2 has 16 O ions per plane and bulk In_2O_3 has 12 O ions per plane in the supercell, while our calculations indicate that the favourable interface oxygen occupation is close to the bulk In_2O_3 value. This is consistent with the fact that In serves as a dopant in ZrO_2 compensated by oxygen vacancies.

We also compared formation energies of an extra oxygen vacancy in different locations of the interface region of a (001) In_2O_3/YSZ heterostructure (see Methods and Supplementary Fig. 8) to provide insight into the feasibility of an electric field causing oxygen vacancies to migrate from YSZ to the In_2O_3 side of the interface region. As seen in Fig. 8b, it is energetically favourable for oxygen vacancies in their lowest energy configurations to move from an oxygen plane in YSZ near the interface to the interface plane or an adjacent oxygen plane in the In_2O_3 film. This will increase the vacancy concentration in In_2O_3, consistent with the experimentally observed doping effect. The predicted localization of vacancies to the In_2O_3/YSZ interface region is also consistent with the experimentally observed film thickness-dependent behaviour discussed above.

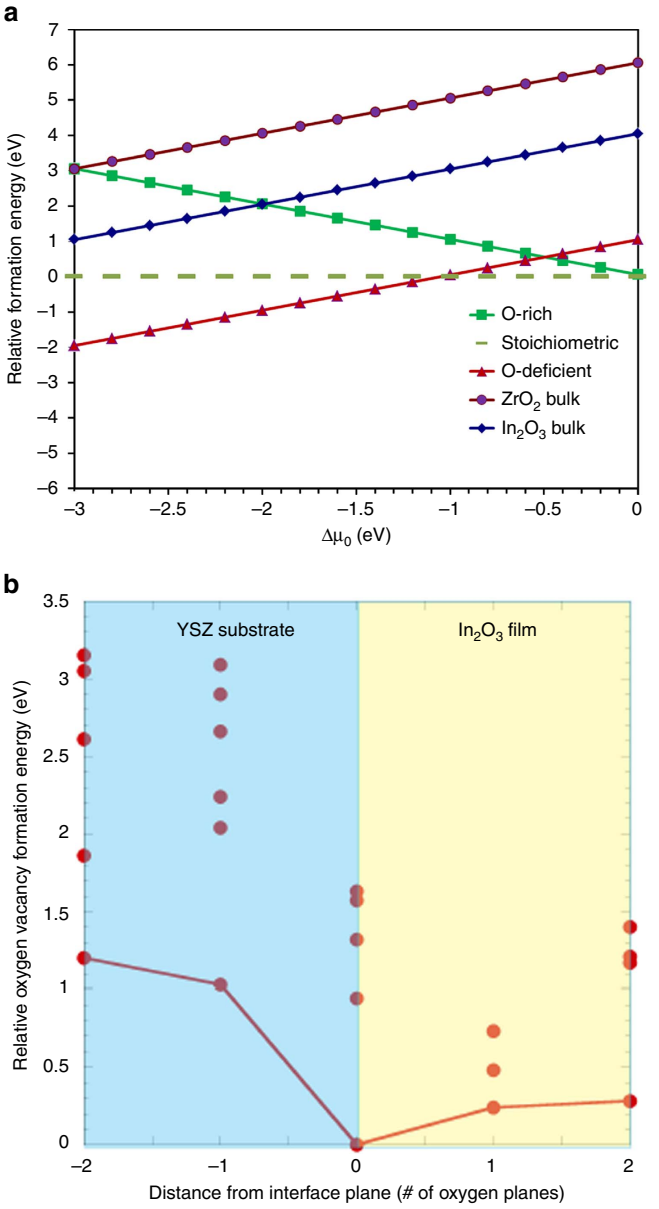

Figure 8 | Oxygen vacancy formation energies. (**a**) Relative formation energy per oxygen vacancy for several interface configurations and bulk vacancies in ZrO_2 and In_2O_3 as a function of oxygen chemical potential relative to molecular oxygen. The zero energy reference is the corresponding stoichiometric structure. (**b**) On the basis of first-principles calculations, the formation energy associated with adding an oxygen vacancy to a YSZ-In_2O_3 supercell is predicted to be significantly lower for sites in the interface plane or adjacent to the interface in the In_2O_3 film than for sites in the YSZ substrate. Energies for multiple possible sites for an oxygen vacancy within each plane are shown. Points connected with a line correspond to the lowest energy positions of the vacancy in each plane. The formation energy values are relative to the energy of the lowest energy site in the heterostructure.

Discussion

The controllable dynamic doping achieved with application of a small lateral (or vertical) electric field demonstrated in this study should be possible in a wide variety of heterostructures. For example, we have also observed similar DC field-induced electrical conduction enhancement in a heterostructure consisting of an epitaxial WO_3 film grown on (001) YSZ (Supplementary Fig. 9). If the heterostructure consists of a film that can be electronically doped by a mobile ion in the substrate, controllable field-driven conductivity should generally be possible. Controllable dynamic doping of the carriers in the electronic conductor can be achieved reversibly, without cation doping or changing the gas environment in contact with the sample, by simply passing a current through the sample parallel to the heterointerface if the field profile in the ionically conducting substrate differs from the profile in the electronically conducting film. This requires that electrode contact resistances in film and substrate are dissimilar, a condition commonly satisfied.

While we have focused in this study on using oxygen vacancy doping to control electrical conduction behaviour in a model thin film heterostructure, we expect that similar heterostructures can be designed and synthesized to control other types of behaviours via oxygen stoichiometry control using small electric fields. The approach of using in-plane electric fields to vary oxygen stoichiometry in heterostructures, which consist of a fast oxygen ion conductor with an electronically conducting functional oxide in a thin film, thus provides a new and unexplored opportunity to tune properties and achieve emergent behaviour.

Methods

Experimental procedures. Epitaxial In_2O_3 films with thicknesses ranging from 4 to 75 nm were deposited by RF sputtering on single crystal (001) or (111) YSZ substrates and on (001) $MgAl_2O_4$ substrates with dimensions $1 \times 1\ cm^2 \times 1$ mm thickness. The substrate temperature was typically 800 °C, and typical growth rates were approximately 10 nm per hour. Sample thickness was characterized using x-ray reflectivity. X-ray diffraction indicated that the films had the expected cube-on-cube orientation relationship (see Supplementary Fig. 10 and Supplementary Note 4). An epitaxial 20 nm thickness WO_3 film was deposited on (001) YSZ, also by RF sputter deposition.

Samples had parallel line Pt electrodes sputter-deposited through a shadow mask onto the film surfaces and, in some cases, on the back surface of the substrate, as shown in Fig. 1. End electrodes were applied using Ag or Pt paint. Most measurements were taken using samples with Ag-painted end electrodes, since bonding of the paint to the sample was generally more reliable (less flaking and measurements were less noisy).

Electrical measurements were taken using an environmental probe station, at controlled T and pO_2. Mass flow controllers were used to mix Ar and O_2 gases to achieve the desired pO_2, at a total chamber pressure of 150 torr. The measurements were taken at $pO_2 = 1.5$ torr, unless otherwise indicated, at temperatures between 300 and 400 °C. DC fields were applied through Pt-coated probe tips in contact with the sample electrodes, using a Keithley Model 2400 source metre. Conduction measurements were typically taken in four-point geometry, with driving current between the end electrodes and conductance measured between a pair of voltage pick-off electrodes on the film surface, under either fixed voltage or fixed current conditions. Contact resistances were measured using a three-electrode geometry with end electrodes 1 and 7 serving as the current source/sink electrodes, with voltage pickoffs at electrodes 1 and 2, or 6 and 7 (Fig. 1). Resistances between electrodes 1 and 2 or between 6 and 7 (10% of total sample resistance) were included in the 3-electrode measurements.

Measurements of the voltage across the In_2O_3/YSZ heterointerface were taken by establishing a fixed current between the end electrodes (Fig. 1), while monitoring the voltage between one electrode on the film surface and another electrode, directly beneath, on the backside of the substrate.

Computational studies. Computational studies used density functional theory within the generalized gradient approximation as implemented in VASP[38,39], with Perdew-Wang exchange-correlation functionals[40] and Projected Augmented Wave potentials[41]. Periodic supercell configurations were analysed, with two interfaces per supercell. Each interface has a shared plane of oxygen ions. As seen in Supplementary Fig. 7, two configurations were considered: (1) a flat In_2O_3 cation plane adjacent to the interface, with In ions occupying two sites (8b and 24d), and (2) a buckled In_2O_3 cation plane adjacent to the interface, with In atoms only occupying 24d sites. In_2O_3-ZrO_2 supercells contained three layers of ZrO_2 and five layers of In_2O_3 (with eight cations in each layer). Structural minimization was performed allowing all the atoms and the supercell in the (001) direction to relax, while keeping the other two dimensions fixed at the bulk value. In_2O_3-YSZ supercells comprised five layers of YSZ and five layers of In_2O_3. Each YSZ cation layer contained six Zr ions and two Y ions, corresponding to a YSZ stoichiometry equivalent to $6ZrO_2$–Y_2O_3. Y ions were distributed in the cell following the approach of a previous computational study[42].

Data availability. The data that support the findings of this study are available from the corresponding author upon request.

References

1. Schladt, T. D. *et al.* Crystal-facet-dependent metallization in electrolyte-gated rutile TiO_2 single crystals. *ACS Nano* **7,** 8074–8081 (2013).
2. Jeong, J. *et al.* Suppression of metal-insulator transition in VO_2 by electric field-induced oxygen vacancy formation. *Science* **339,** 1402–1405 (2013).
3. Younis, A., Chu, D. W. & Li, S. A. Oxygen level: the dominant of resistive switching characteristics in cerium oxide thin films. *J. Phys. D Appl. Phys.* **45,** 355101 (2012).
4. Yang, Y. C., Choi, S. & Lu, W. Oxide heterostructure resistive memory. *Nano Lett.* **13,** 2908–2915 (2013).
5. Brinkman, A. *et al.* Magnetic effects at the interface between non-magnetic oxides. *Nat. Mater.* **6,** 493–496 (2007).
6. Li, L., Richter, C., Mannhart, J. & Ashoori, R. C. Coexistence of magnetic order and two-dimensional superconductivity at $LaAlO_3/SrTiO_3$ interfaces. *Nat. Phys.* **7,** 762–766 (2011).
7. Pavlenko, N., Kopp, T. & Mannhart, J. Emerging magnetism and electronic phase separation at titanate interfaces. *Phys. Rev. B* **88,** 201104 (2013).
8. Pavlenko, N., Kopp, T., Tsymbal, E. Y., Sawatzky, G. A. & Mannhart, J. Magnetic and superconducting phases at the $LaAlO_3/SrTiO_3$ interface: the role of interfacial Ti 3d electrons. *Phys. Rev. B* **85,** 020407 (2012).
9. Salluzzo, M. *et al.* Origin of interface magnetism in $BiMnO_3/SrTiO_3$ and $LaAlO_3/SrTiO_3$ heterostructures. *Phys. Rev. Lett.* **111,** 087204 (2013).
10. Lin, C. W. & Demkov, A. A. Consequences of oxygen-vacancy correlations at the $SrTiO_3$ interface. *Phys. Rev. Lett.* **113,** 157602 (2014).
11. Sase, M. *et al.* Enhancement of oxygen surface exchange at the hetero-interface of $(La,Sr)CoO_3/(La,Sr)_2CoO_4$ with PLD-layered films. *J. Electrochem. Soc.* **155,** B793–B797 (2008).
12. Sase, M. *et al.* Enhancement of oxygen exchange at the hetero interface of $(La,Sr)CoO_3/(La,Sr)_{(2)}CoO_4$ in composite ceramics. *Solid State Ion.* **178,** 1843–1852 (2008).
13. Jeen, H. *et al.* Orienting oxygen vacancies for fast catalytic reaction. *Adv. Mater.* **25,** 6459–6463 (2013).
14. Chen, Y. *et al.* Electronic activation of cathode superlattices at elevated temperatures—source of markedly accelerated oxygen reduction kinetics. *Adv. Energy Mater.* **3,** 1221–1229 (2013).
15. Jalili, H., Han, J. W., Kuru, Y., Cai, Z. H. & Yildiz, B. New insights into the strain coupling to surface chemistry, electronic structure, and reactivity of $La_{0.7}Sr_{0.3}MnO_3$. *J. Phys.l Chem. Lett.* **2,** 801–807 (2011).
16. Crumlin, E. J. *et al.* Surface strontium enrichment on highly active perovskites for oxygen electrocatalysis in solid oxide fuel cells. *Energy Environ. Sci.* **5,** 6081–6088 (2012).
17. Ohtomo, A. & Hwang, H. Y. A high-mobility electron gas at the $LaAlO_3/SrTiO_3$ heterointerface. *Nature* **427,** 423–426 (2004).
18. Chen, Y. *et al.* metallic and insulating interfaces of amorphous $SrTiO_3$-based oxide heterostructures. *Nano Lett.* **11,** 3774–3778 (2011).
19. Bristowe, N. C., Littlewood, P. B. & Artacho, E. Surface defects and conduction in polar oxide heterostructures. *Phys. Rev. B* **83,** 205405 (2011).
20. Liu, Z. Q. *et al.* Origin of the two-dimensional electron gas at $LaAlO_3/SrTiO_3$ interfaces: the role of oxygen vacancies and electronic reconstruction. *Phys. Rev. X* **3,** 031043 (2013).
21. Chen, Y. Z. *et al.* A high-mobility two-dimensional electron gas at the spinel/perovskite interface of gamma-$Al_2O_3/SrTiO_3$. *Nat. Commun.* **4,** 2394 (2013).
22. Lee, S. W., Liu, Y., Heo, J. & Gordon, R. G. Creation and control of two-dimensional electron gas using al-based amorphous oxides/$SrTiO_3$ heterostructures grown by atomic layer deposition. *Nano Lett.* **12,** 4775–4783 (2012).
23. Bierwagen, O. & Speck, J. S. Nucleation of islands and continuous high-quality In_2O_3(001) films during plasma-assisted molecular beam epitaxy on Y-stabilized ZrO_2(001). *J. Appl. Phys.* **107,** 113519 (2010).
24. Bourlange, A. *et al.* Growth of In_2O_3(100) on Y-stabilized ZrO_2(100) by O-plasma assisted molecular beam epitaxy. *Appl. Phys. Lett.* **92,** 092117 (2008).
25. Bourlange, A. *et al.* Investigation of the growth of In_2O_3 on Y-stabilized ZrO_2(100) by oxygen plasma assisted molecular beam epitaxy. *Thin Solid Films* **517,** 4286–4294 (2009).
26. Agoston, P., Albe, K., Nieminen, R. M. & Puska, M. J. Intrinsic n-type behavior in transparent conducting oxides: a comparative hybrid-functional study of In_2O_3, SnO_2, and ZnO. *Phys. Rev. Lett.* **103,** 245501 (2009).
27. Bak, T. *et al.* Electrical conductivity of indium sesquioxide thin film. *J. Mater. Sci.Mater. Electron.* **13,** 571–579 (2002).
28. Norby, T. & Hartmanova, M. Electrical-conductivity and ionic transport number of YSZ and Cr-doped YSZ single-crystals at 200-1000-degrees-C. *Solid State Ion.* **67,** 57–64 (1993).
29. Kröger, F. A. & Vink, H. J. Relations between the concentrations of imperfections in crystalline solids. *Solid State Phys.* **3,** 307–435 (1956).
30. Hörlein, M. P., Opitz, A. K. & Fleig, J. On the variability of oxygen exchange kinetics of platinum model electrodes on yttria stabilized zirconia. *Solid State Ion.* **247-248,** 56–65 (2013).
31. Stancovski, V., Sridhar, S. & Pal, U. B. Thermodynamic stability and interfacial impedance of solid-electrolyte cells with noble-metal electrodes. *J. Electroceram.* **3,** 279–299 (1999).
32. Foti, G., Jaccoud, A., Falgairette & Comninellis, C. Charge storage at the Pt/YSZ interface. *J. Electroceram.* **23,** 175 (2009).
33. Falgairette, C. & Foti, G. Oxygen storage in O_2/Pt/YSZ cell. *Catal. Today* **146,** 274–278 (2009).
34. Siegel, D. A., El Gabaly, F., McCarty, K. F. & Bartelt, N. C. In situ characterization of the formation of a mixed conducting phase on the surface of yttria-stabilized zirconia near Pt electrodes. *Phys. Rev. B* **92,** 125421 (2015).

35. von Wenckstern, H. *et al.* Schottky contacts to In_2O_3. *APL Mater.* **2,** 046104 (2014).
36. Hebb, M. H. Electric conductivity of silver sulfide. *J. Chem. Phys.* **20,** 185–189 (1952).
37. Wagner, C. in *Proceedings of the 7th Meeting of the International Committee of Electrochemical Thermodynamics and Kinetics*, 361 (Butterworths, 1957).
38. Kresse, G. & Furthmuller, J. Efficient iterative schemes for ab initio total-energy calculations using a plane-wave basis set. *Phys. Rev. B* **54,** 11169–11186 (1996).
39. Kresse, G. & Furthmuller, J. Efficiency of ab-initio total energy calculations for metals and semiconductors using a plane-wave basis set. *Comput. Mater. Sci.* **6,** 15–50 (1996).
40. Perdew, J. P. & Wang, Y. Accurate and simple analytic representation of the electron-gas correlation-energy. *Phys. Rev. B* **45,** 13244–13249 (1992).
41. Blochl, P. E. Projector augmented-wave method. *Phys. Rev. B* **50,** 17953–17979 (1994).
42. Predith, A., Ceder, G., Wolverton, C., Persson, K. & Mueller, T. Ab initio prediction of ordered ground-state structures in $ZrO_{(2)}$-$Y_{(2)}O_{(3)}$. *Phys. Rev. B* **77,** 7 (2008).

Acknowledgements

This work was supported by the US Department of Energy, Office of Science, Office of Basic Energy Sciences, Materials Sciences and Engineering Division. We thank Huajun Liu for providing the WO_3-on-YSZ sample used for the measurement shown in Supplementary Fig. 9, and we thank Dillon Fong, Matt Highland, Paul Fuoss and Carol Thompson who participated in the experiments described in Supplementary Note 4. Computer time allocations at the Fusion Computer Facility, Argonne National Laboratory, are gratefully acknowledged.

Author contributions

J.A.E. and B.W.V. conceived and initiated the study. S.K.K., P.M.B. and J.A.E. grew the thin film heterostructures. J.A.E., B.W.V. and S.K.K. performed the experimental measurements. H.I. and P.Z. performed the computational studies. All authors contributed to discussions, data analysis and editing of the paper.

Additional information

Supplementary Information accompanies this paper at http://www.nature.com/naturecommunications

Competing financial interests: The authors declare no competing financial interests.

Reprints and permission information is available online at http://npg.nature.com/reprintsandpermissions/

How to cite this article: Veal, B. W. *et al.* Interfacial control of oxygen vacancy doping and electrical conduction in thin film oxide heterostructures. *Nat. Commun.* 7:11892 doi: 10.1038/ncomms11892 (2016).